

# Neuregulin stimulation of cardiomyocyte regeneration in mice and human myocardium reveals a therapeutic window

Brian D. Polizzotti,<sup>1,2\*</sup> Balakrishnan Ganapathy,<sup>1,3\*</sup> Stuart Walsh,<sup>1,2,\*†</sup> Sangita Choudhury,<sup>1,2,\*</sup> Niyatie Ammanamanchi,<sup>1,3</sup> David G. Bennett,<sup>4‡</sup> Cristobal G. dos Remedios,<sup>5</sup> Bernhard J. Haubner,<sup>6</sup> Josef M. Penninger,<sup>6</sup> Bernhard Kühn<sup>1,2,3,7,8,9§</sup>

Therapies developed for adult patients with heart failure have been shown to be ineffective in pediatric clinical trials, leading to the recognition that new pediatric-specific therapies for heart failure must be developed. Administration of the recombinant growth factor neuregulin-1 (rNRG1) stimulates regeneration of heart muscle cells (cardiomyocytes) in adult mice. Because proliferation-competent cardiomyocytes are more abundant in growing mammals, we hypothesized that administration of rNRG1 during the neonatal period might be more effective than in adulthood. If so, neonatal rNRG1 delivery could be a new therapeutic strategy for treating heart failure in pediatric patients. To evaluate the effectiveness of rNRG1 administration in cardiac regeneration, newborn mice were subjected to cryoinjury, which induced myocardial dysfunction and scar formation and decreased cardiomyocyte cell cycle activity. Early administration of rNRG1 to mice from birth to 34 days of age improved myocardial function and reduced the prevalence of transmural scars. In contrast, administration of rNRG1 from 4 to 34 days of age only transiently improved myocardial function. The mechanisms of early administration involved cardiomyocyte protection (38%) and proliferation (62%). We also assessed the ability of rNRG1 to stimulate cardiomyocyte proliferation in intact cultured myocardium from pediatric patients. rNRG1 induced cardiomyocyte proliferation in myocardium from infants with heart disease who were less than 6 months of age. Our results identify an effective time period within which to execute rNRG1 clinical trials in pediatric patients for the stimulation of cardiomyocyte regeneration.

## INTRODUCTION

Congenital heart disease (CHD) is the leading cause of birth defect-related morbidity and mortality (1, 2). Although corrective surgery enables young patients to survive most forms of CHD, they are at risk of developing chronic heart failure (3). The currently available therapies for heart failure—such as  $\beta$ -blockers and angiotensin-converting enzyme inhibitors—were developed for adult patients, but subsequently were shown to be ineffective in controlled pediatric trials (4–6). There is an increasing awareness that the underlying mechanisms of heart failure are different in pediatric patients than in adults, and thus new therapeutic paradigms must be developed (4).

The goal of cardiac regeneration is to provide new functionally integrated heart muscle cells (cardiomyocytes). Three principal strategies are being pursued: transplantation of stem cells, transdifferentiation of fibroblasts into cardiomyocytes, and stimulation of endogenous cardiomyocyte proliferation (7, 8). Although human adults show little or no endogenous cardiomyocyte proliferation, this does not seem to be

true for younger people under 20 years of age (9, 10). In fact, cardiomyocyte proliferation contributes to physiological heart growth in young humans (10). Cardiomyocyte proliferation during postnatal heart growth was also shown in mouse and rat pups, but proliferation declines significantly during the first week of life (11, 12). The rate of endogenous cardiomyocyte proliferation is higher in neonatal mice (1 to 4 days after birth) than in preadolescent mice (14 to 18 days after birth) and adult mice (60 days after birth) (11, 13, 14). Neonatal mice were reported to be capable of scarless regeneration (15–17), in contrast to preadolescent mice, which can only partially regenerate after myocardial injury (14). Although endogenous cardiomyocyte proliferation can be detected in humans without heart disease up to 20 years of age (10), the presence of heart disease likely influences the rate of cardiomyocyte proliferation.

Neuregulin-1 (NRG1), a member of the epidermal growth factor family, is required for cardiac development (18, 19) and for limiting injury after myocardial ischemia (20). Administration of recombinant NRG1 (rNRG1) preparations is beneficial in a variety of small and large animal models of acquired heart disease (21–24). rNRG1 is currently being pursued as an investigational new drug for the treatment of heart failure (25, 26) and has been shown to be effective in adult patients with a left ventricular ejection fraction (LVEF) <40% (27, 28). Thus, rNRG1 is available and suitable for administration in humans.

Different mechanisms of action have been proposed to explain the beneficial effects of rNRG1 administration in heart failure (29, 30). Because rNRG1 stimulates cardiomyocyte proliferation (22, 24, 29, 30), it has the potential to benefit pediatric patients. Here, we combine heart regeneration experiments in neonatal mice with cell biological experiments in intact human myocardium to characterize the period of cardiomyocyte proliferation, the ability to stimulate proliferation

<sup>1</sup>Department of Cardiology, Boston Children's Hospital, Boston, MA 02115, USA. <sup>2</sup>Department of Pediatrics, Harvard Medical School, Boston, MA 02115, USA. <sup>3</sup>Department of Pediatrics, University of Pittsburgh, and Richard King Mellon Institute for Pediatric Research and Division of Pediatric Cardiology, Children's Hospital of Pittsburgh of UPMC, Pittsburgh, PA 15224, USA. <sup>4</sup>Preclinical MRI Core, Beth Israel Deaconess Medical Center, Boston, MA 02115, USA. <sup>5</sup>Department of Anatomy, Bosch Institute, The University of Sydney, Sydney, New South Wales 2006, Australia. <sup>6</sup>Institute of Molecular Biotechnology of the Austrian Academy of Sciences, 1030 Vienna, Austria. <sup>7</sup>Harvard Stem Cell Institute, Cambridge, MA 02138, USA. <sup>8</sup>Department of Stem Cell and Regenerative Biology, Harvard University, Cambridge, MA 02138, USA. <sup>9</sup>McGowan Institute for Regenerative Medicine, Pittsburgh, PA 15219, USA.

\*These authors contributed equally to this work.

†Present address: Bayer Healthcare, 42096 Wuppertal, Germany.

‡Present address: PAREXEL Informatics, Billerica, MA 01821, USA.

§Corresponding author. E-mail: bernhard.kuhn2@chp.edu

with rNRG1, and the relationship between the timing of rNRG1 administration and myocardial repair.

## RESULTS

### Cryo-injury in neonatal mice induces myocardial cell death

We used cryoinjury to create a neonatal mouse model of myocardial dysfunction and scarring and emulated key elements of previously published amputation and cryoinjury methods used in zebrafish (31–34) and in neonatal mice (35, 36). We fashioned a metal cryoprobe, cooled it in liquid nitrogen for ~20 min, and applied it to the surface of the heart for 2 s. Using this technique, we performed more than 500 surgeries on the first day of life (P1) and observed a 24-hour mortality of 20% and a mortality of 25% between 24 hours and 7 days post-injury (dpi). Mortality was largely associated with maternal cannibalism.

Having implemented a feasible and survivable injury technique, we examined the extent and degree of tissue injury achieved by cryoinjury. Bright-field microscopy showed superficial hemorrhages at 1 dpi (Fig. 1A), and vital staining with triphenyltetrazolium chloride (TTC) demarcated the injured region on the surface of the heart (Fig. 1B). The extent of myocardial death was visualized by terminal deoxynucleotidyl transferase-mediated deoxyuridine triphosphate nick end labeling (TUNEL) staining on histological sections (Fig. 1C). The TUNEL-positive myocardial volume at 1 dpi was  $0.58 \pm 0.02 \text{ mm}^3$  ( $n = 6$ ), corresponding to ~18% of the myocardium (Fig. 1D). Staining with a sarcomeric marker revealed disorganized sarcomeres and an overall decreased abundance of sarcomeric proteins in the cryoinjured area (fig. S2).

### Cryo-injury induces myocardial dysfunction and scarring

We performed echocardiography to examine the degree and time course of myocardial dysfunction after cryoinjury on P1. The left ventricular ejection fraction (LVEF) decreased in the control hearts between 4 and 14 dpi (Fig. 1E), consistent with the previously reported decrease in contractility within this age range (37). Cryoinjury reduced the EF significantly at all time points examined. As an example, at 30 dpi, the EF in the cryoinjury group was  $45.7 \pm 3\%$  ( $n = 19$ ) compared to  $57.9 \pm 3.5\%$  ( $n = 19$ ;  $P < 0.05$ , ANOVA) in sham mice. Thus, cryoinjury induced significant and sustained myocardial dysfunction.

We also examined the extent and time course of myocardial injury and observed fibrin deposition at 1 dpi and significant fibrosis at 7 dpi, which matured into transmural scars (that is, the radial myocardial wall dimension is composed of scar) at 30 dpi (Fig. 1F and fig. S3). We followed a group of mice for 7 months after cryoinjury, and they all showed transmural scars ( $n = 6$ ; Fig. 1G and fig. S4). Morphometric analysis revealed that the relative scar volume after neonatal cryoinjury was comparable to values obtained after ligation of the left anterior descending artery (LAD ligation) in adult mice, which means that the amount of scar produced after neonatal cryoinjury is equal to that produced after experimental myocardial infarction in adult mice (Fig. 1H) (22). In summary, cryoinjury in neonatal mouse hearts on P1 induced persistent myocardial dysfunction and scar formation.

### Cryo-injury reduces cardiomyocyte cycling

Our data demonstrated a lack of significant regeneration at the structural (scar, Fig. 1F) and functional levels (echocardiography, Fig. 1E) and raise the question of whether there is evidence of cardiac regeneration at the cellular level. Because cardiomyocyte cell cycle activity was

shown to increase with myocardial regeneration in zebrafish (38) and neonatal mice (15, 16), we evaluated this mechanism by visualizing cardiomyocytes in karyokinesis using an anti-phospho-histone H3 (H3P) antibody. In sham-operated and cryoinjured hearts, the overall number of H3P-positive cardiomyocytes decreased significantly between 1 and 7 dpi (Fig. 1, I and J), consistent with prior studies showing that cardiomyocyte cell cycle activity decreases in the first week of life (11, 12). However, the numbers of H3P-positive cardiomyocytes in the injury and border zones were significantly lower in cryoinjured hearts at 1, 4, and 7 dpi compared with the corresponding region in sham-operated hearts (Fig. 1J). These results indicate that cryoinjury in neonatal mice inhibits endogenous cardiomyocyte cell cycle activity and, thus, that neonatal hearts do not regenerate to the same degree after cryoinjury as reported for hearts after myocardial resection or LAD ligation (15, 17).

### Administration of rNRG1 improves myocardial function

Because administration of rNRG1 stimulates cardiomyocyte cycling and proliferation *in vitro* and myocardial repair *in vivo* (22, 24, 29, 30), we investigated the effect of rNRG1 on cardiomyocyte cycling in our cryoinjury mouse model. Toward this goal, we performed two independent pre-clinical studies in which only the beginning of rNRG1 therapy was varied (schematic shown in Fig. 2A). In both experiments, cryoinjury was induced 1 day after birth in all animals, with control animals receiving daily injections of bovine serum albumin (BSA) and test animals receiving daily injections of rNRG1 (100 ng/g). In the first study (referred to as “early administration” from here on), therapy began at birth and continued every day for 34 days. These mice showed a significant improvement in their EF (measured by echocardiography) beginning at 5 dpi (Fig. 2B). The absolute improvement of the EF was increased by 14 dpi and persisted for 30 days (64 dpi) after cessation of rNRG1 administration. Cardiac magnetic resonance imaging (cMRI), performed by a blinded core laboratory at 64 dpi, showed an increase of the EF from  $44.3 \pm 2.7$  ( $n = 6$ ) in BSA-treated mice to  $58.3 \pm 1$  ( $n = 5$ ;  $P < 0.0001$ , Student's *t* test) in rNRG1-treated mice, in agreement with the echocardiography results (Fig. 2C, fig. S5, and movies S1 and S2). The relative heart weights were significantly lower in rNRG1-treated mice at 64 dpi (Fig. 2D), indicating that rNRG1 administration induced beneficial changes in the myocardium that persisted for 30 days after cessation of therapy.

In the second study (referred to as “late administration” from here on), we began therapy at 5 days after birth (4 dpi) and kept the remainder of the experimental design the same. Echocardiography showed a significant increase in the EF, first observed at 14 dpi (Fig. 2E). However, at 64 dpi (that is, 30 days after cessation of rNRG1 injections), echocardiography and cMRI showed that the EF was no longer different between BSA- and rNRG1-treated mice (Fig. 2, E and F, fig. S6, and movies S3 and S4). There also were no significant changes in heart weight after late administration (Fig. 2G). In summary, early administration of rNRG1 yielded sustained improvements in cardiac function, leading to the conclusion that the timing of rNRG1 therapy is important for long-term results.

### Early administration of rNRG1 prevents transmural scar formation

We examined histological sections for scar formation at 10, 34, and 64 dpi (Fig. 2H and figs. S7 and S8). Quantification of the scar size at 10 dpi showed a statistically significant decrease in rNRG1-treated mice after early administration but not after late administration (Fig. 2, I and J). The relative scar size at 64 dpi (that is, when mice reached adult age) was ~2.5% after early and late administration (Fig. 2, I

and J), which is comparable to our measurements in adult mice after LAD ligation (22). At 34 and 64 dpi after early administration of rNRG1, only one heart showed a transmural scar ( $n = 10$ ; Fig. 2K).

In contrast, 76.5% of mice starting rNRG1 late ( $n = 12$ ) or receiving BSA ( $n = 22$ ) showed transmural scars at 34 and 64 dpi ( $P = 0.0003$ , Fisher's exact test on raw data; Fig. 2K). In conclusion, early rNRG1

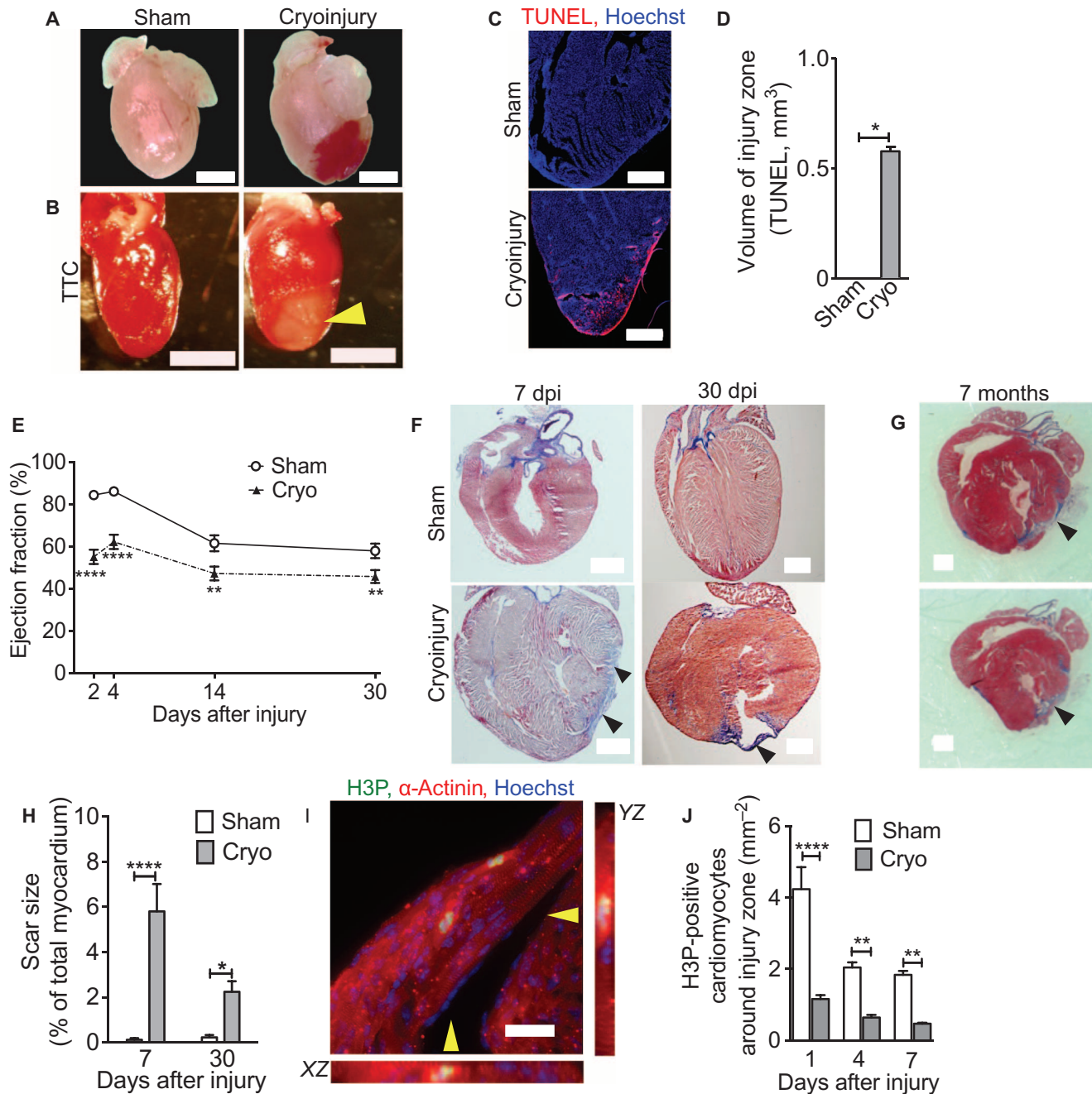


**Fig. 1. Cryoinjury induces cell death, myocardial dysfunction, and decreased cardiomyocyte cell cycle activity in neonatal mice.** Mice underwent sham surgery or cryoinjury on P1. (A) Hematoma at the injury site. (B) Vital staining with TTC shows the injury zone indicated by yellow arrowhead. (C and D) Myocardial cell death visualized by TUNEL staining (red) and DNA staining with Hoechst (blue) (C) and quantification (D). (E) Cryoinjury induces a sustained decrease in EF. (F) Acid fuchsin–orange G (AFOG)–stained sections show scar (blue) formation (within 7 dpi and present 30 days later). (G) Cryoinjury-induced scars, visualized on two sections of the same heart (500  $\mu\text{m}$  apart) by Masson trichrome staining, persist to 7 months after injury.

(H) Quantification of scar size. (I) Two cardiomyocytes in M phase visualized with antibodies against H3P (green/yellow),  $\alpha$ -actinin (red), and Hoechst (blue). The position of orthogonal reconstructions (along the XZ and YZ axes) of the cardiomyocyte in the center are indicated by yellow arrowheads. (J) Quantification of M-phase cardiomyocytes in the region around the injury zone shows significant and sustained reduction after cryoinjury. Scar region is indicated by black arrowheads (F and G). Scale bars, 1 mm (A, B, F, and G) and 20  $\mu\text{m}$  (C and I). Statistical analysis by Student's  $t$  test (D) and analysis of variance (ANOVA) followed by Bonferroni's multiple comparison test (E, H, and J). \* $P < 0.05$ , \*\* $P < 0.01$ , \*\*\* $P < 0.001$ , \*\*\*\* $P < 0.0001$ . Cryo, cryoinjury.

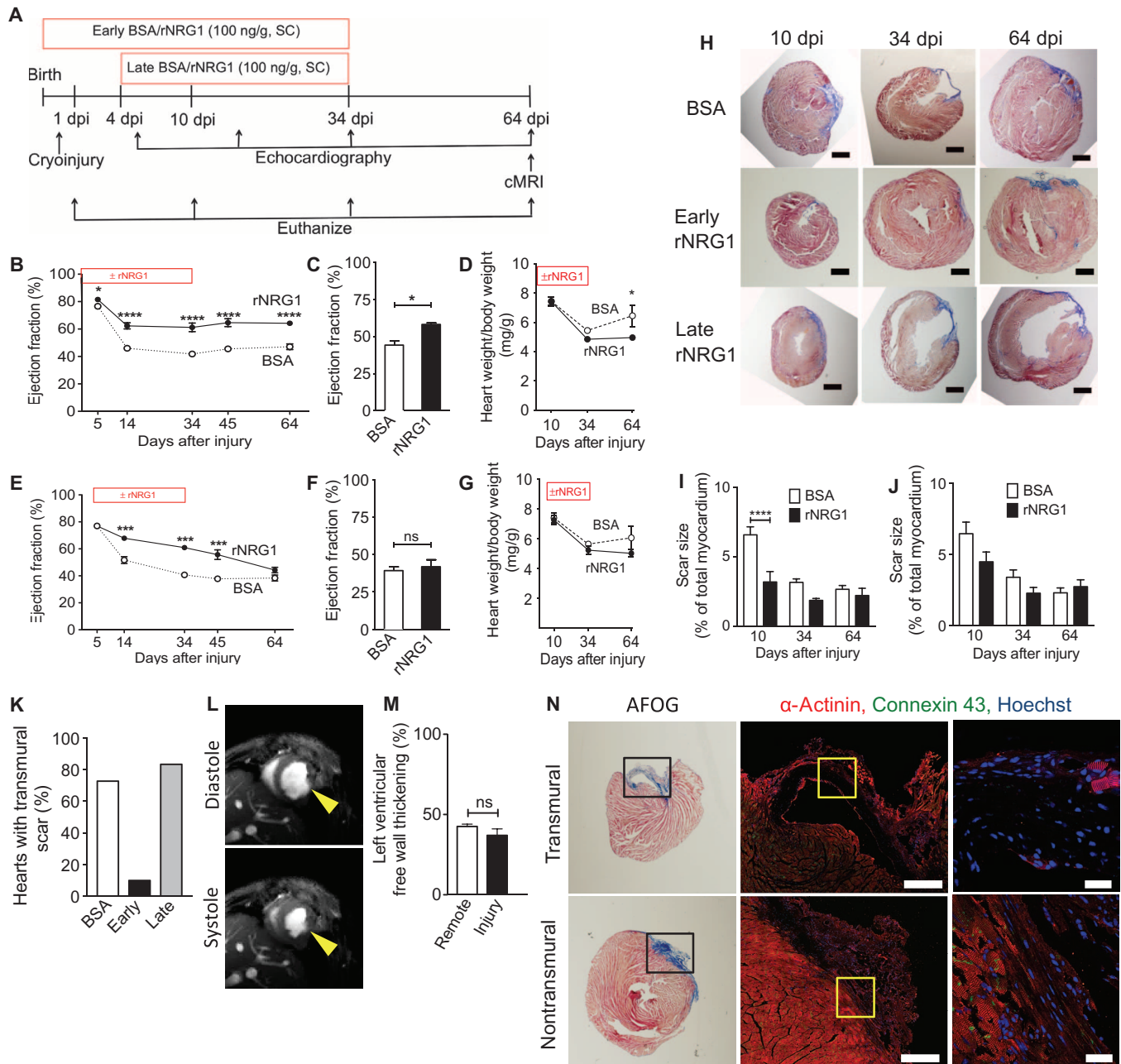


**Fig. 2. Early administration of rNRG1 improves myocardial function and structure.** (A) Experimental design of mouse preclinical trials. (B to N) Mice underwent cryoinjury on P1 and were treated with BSA or rNRG1 from P0 (early administration; B to D) or from P5 (late administration; E to G). Prolonged improvement in myocardial function after early administration shown by echocardiography (B) and cMRI at 64 dpi (C). Late administration of rNRG1 resulted in transient improvement of myocardial function measured by echocardiography (E) and cMRI at 64 dpi (F). (D and G) Indexed heart weights showed that early rNRG1 administration reduced cardiac hypertrophy at 64 dpi. (H) Time series of AFOG-stained section shows that scar (blue) is formed within 10 dpi and is still present at 64 dpi. Note transmural scars after cryoinjury in BSA and late-administration rNRG1 treatment groups. Quantification of scar size after AFOG staining shows transient and significant scar reduction after early rNRG1 administration (I) when compared to late administration (J). (K) Early administration reduces the percentage of transmural scars at 34 and 64 dpi. (L) Nontransmural injury site thickens in systole (64 dpi, early administration). (M) Relative thickening of nontransmural scars is similar to remote LV free wall myocardium. (N) Transmural and nontransmural scars were identified by AFOG sections (left panels). Black rectangles indicate photomicrographs shown in the middle panels. Nontransmural scars have cardiomyocytes connected by gap junctions visualized with connexin 43 staining (64 dpi, early administration; middle and right panels). Yellow squares indicate zoomed-in areas of scar region (right panels). Scale bars, 1 mm (H), 500 μm (N, center panel), and 50 μm (N, far right). SC, subcutaneous injection. Statistical significance was tested with Student's *t* test (C, F, and M), ANOVA followed by Bonferroni's multiple comparison test (B, D, E, G, I, and J), and Fisher's exact test (K). \**P* < 0.05, \*\**P* < 0.01, \*\*\**P* < 0.001, \*\*\*\**P* < 0.0001; ns, not significant.

pared to late administration (J). (K) Early administration reduces the percentage of transmural scars at 34 and 64 dpi. (L) Nontransmural injury site thickens in systole (64 dpi, early administration). (M) Relative thickening of nontransmural scars is similar to remote LV free wall myocardium. (N) Transmural and nontransmural scars were identified by AFOG sections (left panels). Black rectangles indicate photomicrographs shown in the middle panels. Nontransmural scars have cardiomyocytes connected by gap junctions visualized with connexin 43 staining (64 dpi, early administration; middle and right panels). Yellow squares indicate zoomed-in areas of scar region (right panels). Scale bars, 1 mm (H), 500 μm (N, center panel), and 50 μm (N, far right). SC, subcutaneous injection. Statistical significance was tested with Student's *t* test (C, F, and M), ANOVA followed by Bonferroni's multiple comparison test (B, D, E, G, I, and J), and Fisher's exact test (K). \**P* < 0.05, \*\**P* < 0.01, \*\*\**P* < 0.001, \*\*\*\**P* < 0.0001; ns, not significant.

administration prevents transmural scar formation without affecting the total volume of scar tissue.

### Nontransmural scars contract and contain cardiomyocytes with electromechanical connections

We examined the functionality of the myocardium in nontransmural scars by cMRI (Fig. 2L). To this end, we measured the thickness of nontransmural scars in the relaxed (diastole) and contracted (systole) states and calculated relative myocardial thickening, a measurement of myocardial function (Fig. 2M). The thickening of nontransmural injury sites was similar to the corresponding remote LV free wall myocardium (Fig. 2M). In contrast, the thickness of transmural scars in the late rNRG1 and BSA groups was so low that it could not be measured, even after enhancement by gadolinium injection, which highlights scar tissue (fig. S9).

We then examined the extent to which cardiomyocytes in nontransmural scars exhibited gap junctions, which are structures that provide electromechanical connections between adjacent cells. We visualized gap junctions with an antibody against connexin 43 (a key structural protein of gap junctions) (Fig. 2N) and found that transmural scars did not contain gap junctions (Fig. 2N, upper panels, and movie S5). In contrast, nontransmural scars had intact myocardium and gap junctions (Fig. 2N, lower panels, and movie S5). These results show that early administration of rNRG1 induces the formation of functionally active myocardium.

### Early administration of rNRG1 preserves myocardium

Because early administration of rNRG1 began before cryoinjury, we considered a cardioprotective effect. The size of the hematoma demarcating the contact site between the myocardium and the cryoprobe was similar in control and rNRG1-treated mice, indicating that the extent of initial injury was not affected by rNRG1 (Fig. 3, A and B). However, at 1 dpi, mice treated with BSA had  $0.88 \pm 0.04 \text{ mm}^3$  ( $n = 6$ ) TUNEL-positive myocardium and rNRG1-treated mice had  $0.51 \pm 0.07 \text{ mm}^3$  ( $n = 5$ ) TUNEL-positive myocardium, representing a significant decrease ( $P = 0.0009$ , Student's  $t$  test; Fig. 3, C and D). The difference (that is,  $0.37 \text{ mm}^3$  at 1 dpi) represents the myocardium protected by rNRG1 and corresponds to 13.6% of the heart. Assuming that  $\sim 1 \times 10^6$  cardiomyocytes exist in the heart at birth (14), rNRG1 rescues  $\sim 136,000$  cardiomyocytes at 1 dpi (Supplementary Results). This suggests that the first two rNRG1 injections of the early administration protocol elicited a small cardioprotective effect.

### Administration of rNRG1 stimulates cardiomyocyte cell cycling

Because rNRG1 increases cardiomyocyte cell cycling *in vitro* (29, 30) and *in vivo* (22, 24), we examined the effect of rNRG1 on the cell division cycle in the cryoinjured mouse neonates by quantifying the number of H3P-positive cardiomyocytes on histological sections (Fig. 3, E to G). Early administration of rNRG1 induced a twofold increase in H3P-positive cardiomyocytes compared with BSA-injected animals at 1 and 10 dpi (Fig. 3F). Late administration of rNRG1 showed a similar effect at 10 dpi (Fig. 3G); however, the increase in cardiomyocyte cycling started 5 days later relative to the animals that received rNRG1 early administration. We examined histological sections for evidence of cardiomyocyte mitosis at 1 dpi and found a significant increase in the number of Aurora B kinase-positive cells in rNRG1 early treated animals (Fig. 3, H and I). These findings show that rNRG1 increases cardiomyocyte mitosis.

### Early administration of rNRG1 stimulates significant cardiomyocyte regeneration in the first 10 days of life

We used stereology to quantify cardiomyocyte nuclei on  $\alpha$ -actinin- and Hoechst-stained sections. Early administration of rNRG1 induced an 18% increase in cardiomyocyte nuclei density compared to BSA-treated mice at 64 dpi (Fig. 3J). We correlated these directly determined stereology results with the predicted number of regenerated cardiomyocytes using our cell cycle data (H3P) and a linear regression model. We then calculated the difference in cardiomyocyte volume density (in  $\text{mm}^{-3}$ ) between BSA- and rNRG1-treated mice for six age bins between birth and 34 days of age and plotted the rNRG1-induced increase for each bin (Fig. 3K and Supplementary Results). Between 1 and 10 dpi, there was a steep slope for the rNRG1-induced increase in the number of cardiomyocytes (slope, 3661 cardiomyocytes/ $\text{mm}^3$  per day; Fig. 3K). In other words, rNRG1 treatment stimulated the generation of  $\sim 36,610$  additional cardiomyocytes/ $\text{mm}^3$  during the first 10 days of life. This accounts for  $\sim 78\%$  of the total number of new cardiomyocytes generated during this period. After 10 days of life, the rate of rNRG1-stimulated cardiomyocyte proliferation declined significantly to  $\sim 96$  cardiomyocytes/ $\text{mm}^3$  per day, resulting in 2,300 new cardiomyocytes/ $\text{mm}^3$  generated between days 10 and 34. These calculations indicate that rNRG1-stimulated cardiomyocyte proliferation in mice was most active in the first 10 days of life (Fig. 3K). In summary, both the timing of rNRG1 administration and the animal age [P0 (day of birth) to P5] are critical determinates of the ability to regenerate myocardium.

### ErbB4 expression in cardiomyocytes is required for rNRG1-stimulated cardiomyocyte cell cycling

We showed previously that adult cardiomyocytes require the receptor tyrosine kinase ErbB4 for rNRG1-stimulated cycling (22). However, it is possible that, in neonatal hearts, rNRG1 also acts on stem or progenitor cells via ErbB4. To explore this possibility, we used *ErbB4* floxed mice to inactivate the NRG1 receptor gene (*ErbB4*) in cardiomyocytes. We administered tamoxifen in  $\alpha$ MHC-MerCreMer; *ErbB4*<sup>F/W<sup>T</sup></sup> mice (control group) and in  $\alpha$ MHC-MerCreMer; *ErbB4*<sup>F/F</sup> mice (test group) from P0 to P3, which led to a significant reduction in *ErbB4* mRNA levels (Fig. 4A). We then quantified H3P-positive cardiomyocytes at P12 and found that rNRG1 increased the number of H3P-positive cardiomyocytes in control mice ( $n = 3$ ) but not in test mice ( $n = 3$ ), indicating that ErbB4 is required for rNRG1-stimulated cardiomyocyte cell cycling (Fig. 4, B and C). Collectively, these data indicate that rNRG1 acts directly on cardiomyocytes, rather than stem cells, via ErbB4 to induce the cell division cycle.

### Cryoinjury and rNRG1 administration induce gene regulation patterns that are consistent with structural and functional changes

We next investigated changes in gene expression profiles induced by cryoinjury and rNRG1 administration. To this end, we induced cryoinjury on P1 and performed RNA sequencing (RNAseq) after early administration of BSA ( $n = 5$ ) or rNRG1 ( $n = 5$ ). Compared with sham ( $n = 5$ ), cryoinjury ( $n = 5$ ) was correlated with a change in the expression of 2,867 genes. We examined a heat map of 622 genes that were regulated in a significantly different manner in the BSA- and rNRG1-treated groups relative to sham-operated mice ( $P < 0.05$ , Cuffdiff; Fig. 5A and table S1). Genes that were significantly up-regulated ( $P < 0.05$ ) by rNRG1 treatment included cyclic adenosine monophosphate-dependent transcription factor 3 (ATF3), geminin (Gmnn), centromere protein A

(Cenpa), growth differentiation factor 15 (GDF15), connective tissue growth factor (Ctgf), and apelin (Apln). In addition, gap junction protein  $\gamma 2$  (Gjc2) was up-regulated in rNRG1-treated hearts, consistent

with our finding that early administration of rNRG1 induced the formation of functional myocardium. Genes that were significantly down-regulated ( $P < 0.05$ ) included collagen 23 $\alpha 1$  (Col23a1), suppressor

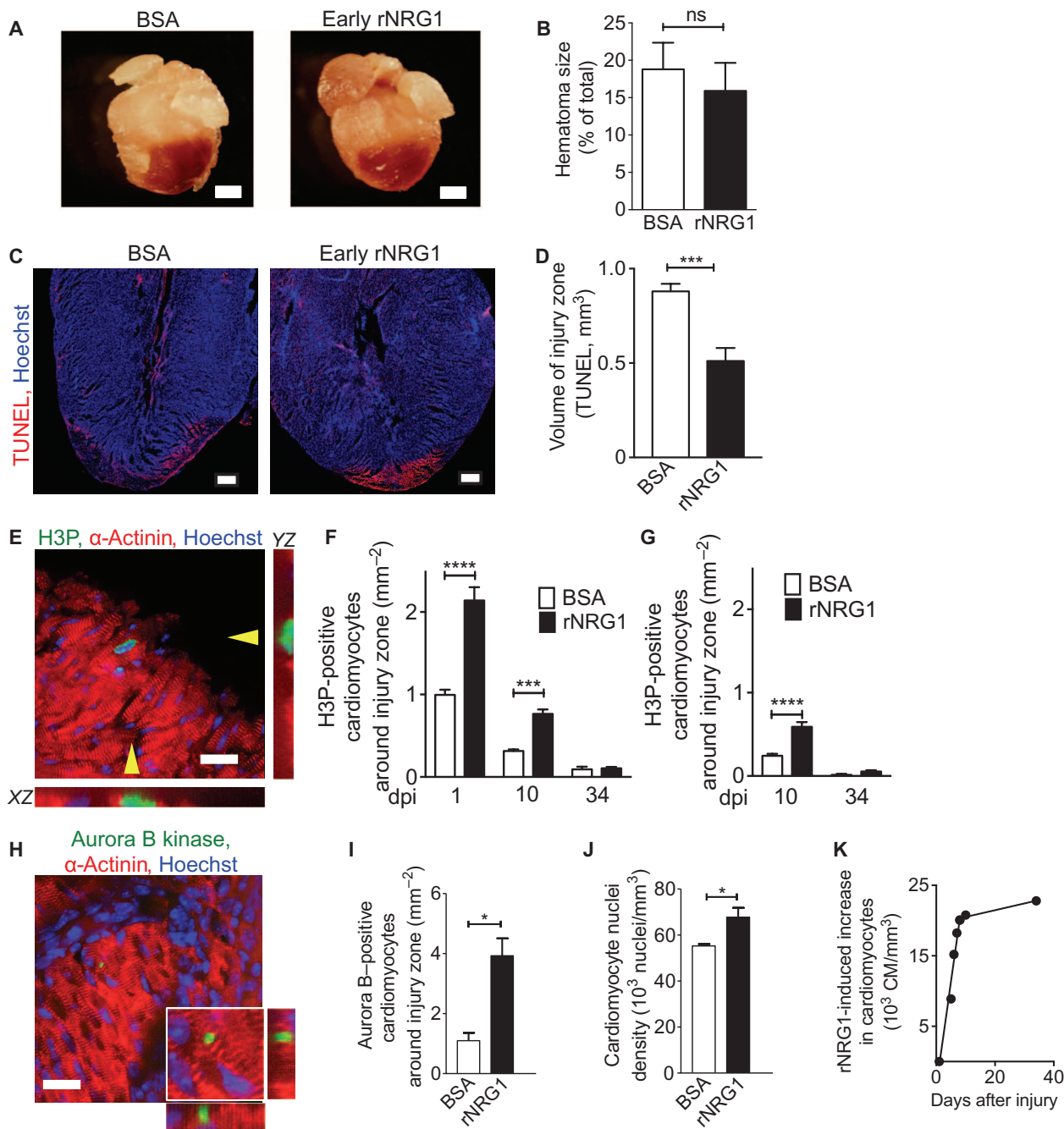


**Fig. 3. Early administration of rNRG1 reduces myocardial death and stimulates cardiomyocyte proliferation.** (A) Hematomas are present at the zone of injury at 1 dpi. (B) Hematoma size quantification shows no change after early administration of rNRG1. (C and D) Photomicrographs (C) and quantification (D) of myocardial cell death visualized by TUNEL staining at 1 dpi after early administration. (E) Cardiomyocytes in M phase were visualized with an antibody against H3P. (F and G) H3P-positive cardiomyocytes were quantified around the injury zone after early (F) and late (G) administration of rNRG1. Treatment with rNRG1 increases cardiomyocyte cell cycle activity, and early administration captures the

regenerative phase (F). (H and I) Cardiomyocytes in cytokinesis were visualized with an antibody against Aurora B kinase (H) and quantified around the injury zone after early administration at 1 dpi (I). (J) Cardiomyocyte nuclear density is increased after early administration of rNRG1 (34 dpi). (K) Early administration of rNRG1 increases the cardiomyocyte density by ~62,000 cardiomyocytes/mm<sup>3</sup> within the first 8 days, compared to BSA controls. CM, cardiomyocytes. Scale bars, 1 mm (A) and 20  $\mu$ m (C, E, and H). Statistical significance was tested with Student's *t* test (B, D, I, and J) and ANOVA followed by Bonferroni's multiple comparison test (F and G). \* $P < 0.05$ , \*\*\*\* $P < 0.001$ , \*\*\*\*\* $P < 0.0001$ ; ns, not significant.

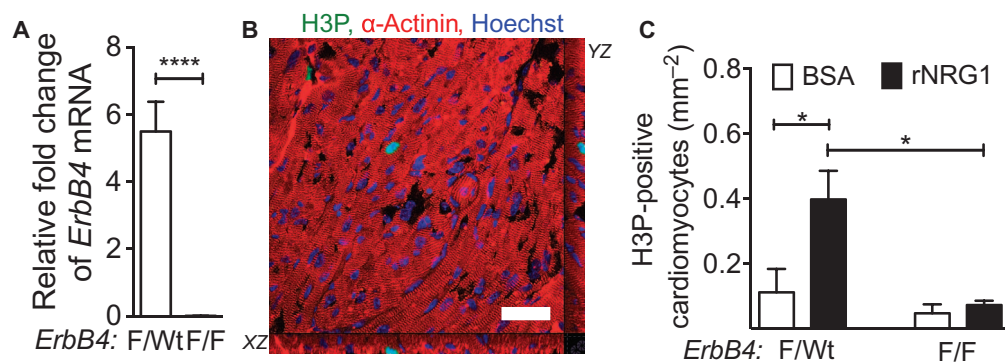


**Fig. 4. rNRG1 acts through ErbB4 on cardiomyocytes in neonatal mouse hearts in vivo.** (A to C) Experiments were performed in  $\alpha$ MHC-MerCreMer<sup>+/+</sup>; ErbB4<sup>F<sup>WT</sup></sup> (control) and  $\alpha$ MHC-MerCreMer<sup>+/+</sup>; ErbB4<sup>F/F</sup> (test) mice. rNRG1 or BSA was administered from P0 until P12. ErbB4 inactivation was induced with tamoxifen administration from days P1 to P3, which caused a significant down-regulation of ErbB4 mRNA levels (A). Representative example of a cardiomyocyte in M phase with orthogonal reconstructions along the XZ and YZ axes (shown by staining of heart sections with an antibody against H3P, B). Quantification of these sections showed that rNRG1 increased cardiomyocyte cell cycle activity in ErbB4<sup>F<sup>WT</sup></sup> but not in ErbB4<sup>F/F</sup> mice (C). Statistical test by Student's *t* test (A) and ANOVA followed by Bonferroni's multiple comparison test (C). \**P* < 0.05, \*\*\*\**P* < 0.0001. Scale bar, 50  $\mu$ m.

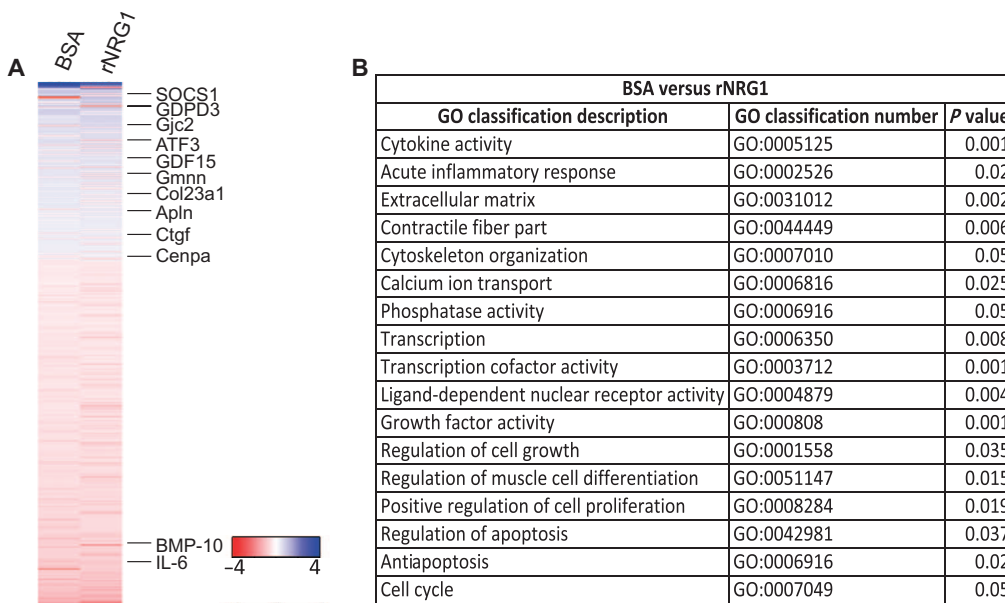


**Fig. 5. Cryoinjury and rNRG1 administration induce gene regulation patterns that are consistent with structural and functional changes.** Mice underwent cryoinjury on P1 and were treated with BSA or rNRG1 according to the early administration protocol. Expression profiling was performed at 10 dpi with five mice per group and were normalized to sham (*n* = 5). (A) Heat map shows 622 genes whose expression was significantly different (*P* < 0.05, Cuffdiff) in BSA- and rNRG1-treated mice relative to sham-operated mice. Selected genes discussed in the text are indicated. The color chart indicates fold change of expression using a log<sub>2</sub> scale. (B) Functional annotation clustering of differentially expressed genes shows significant differences in the expression of components of multiple biological pathways by rNRG1. GO, Gene Ontology, a major bioinformatics initiative to unify the representation of gene and gene product attributes enabling functional interpretation of experimental data through enrichment analysis. *P* values were generated by DAVID bioinformatics tools. Fisher's exact test was adopted to measure gene enrichment in annotation terms.

of cytokine signaling 1 (SOCS1), bone morphogenic protein 10 (BMP-10), interleukin-6 (IL-6), and glycerophosphodiester phosphodiesterase domain-containing protein 3 (GPPD3). Functional annotation clustering revealed that the genes whose expression changed with rNRG1 treat-

ment encoded cytokines, cell growth and division regulators, and transcription factors (Fig. 5B). In summary, the broad changes in gene regulation paralleled the observed functional and structural changes.

**Cardiomyocyte cell cycling is decreased in pediatric patients with heart disease**

The results from our mouse studies suggest that rNRG1 therapy is most effective during an early-administration therapeutic period. To determine whether a similar trend is present in humans, we examined myocardium obtained from patients with heart disease (for clinical characteristics, see tables S2 and S3). Although cardiomyocyte proliferation occurs in humans without heart disease up to 20 years of age, the presence of heart disease might influence cardiomyocyte cell cycle activity. We isolated cardiomyocytes from patient samples, stained them with antibodies against pan-cadherin to determine cell quality (Fig. 6A), and then used flow cytometry to quantify the population of cardiomyocytes that were H3P-positive; H3P-positive cardiomyocytes were detected in patients younger than 6 months but not in patients older than 6 months (Fig. 6, B and C). Furthermore, cardiomyocytes from patients with heart disease exhibited lower cell cycle activity compared to nondiseased myocardium (Fig. 6C). Together, these findings suggest that pediatric patients with heart disease exhibit lower levels and earlier cessation of cardiomyocyte cell cycle activity relative to pediatric donor hearts without disease.

**Infants with heart disease have the capacity for stimulated cardiomyocyte cycling**

We tested whether rNRG1 therapy could stimulate the cycling of cardiomyocytes from patients with heart disease. To accomplish this, we modified an organotypic cell culture system for primary human myocardium

(39). A parallel sheet-like arrangement of cardiomyocytes, sarcomeric striations (Fig. 7A), and gap junctions (Fig. 7B) were present after 72 hours of organotypic culture. Thus, the organotypic culture represents a three-dimensional (3D) multicellular model of the human myocardium and

Downloaded from [stm.sciencemag.org](http://stm.sciencemag.org) on April 1, 2015

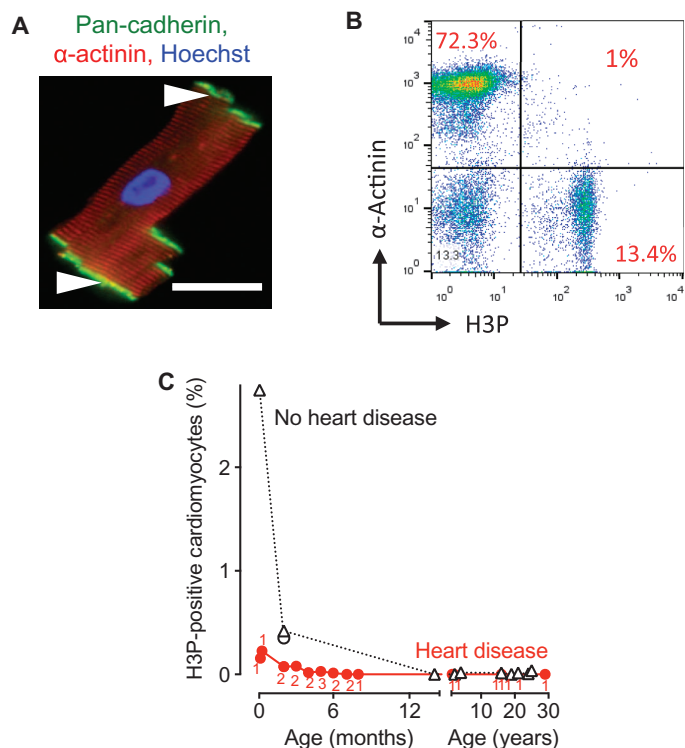


**Fig. 6. Pediatric patients with heart disease show decreased cardiomyocyte cell cycle activity.** Cardiomyocytes from patients were isolated, stained, and analyzed by flow cytometry. **(A)** Isolated human cardiomyocytes were intact as evidenced by staining with antibodies to pan-cadherin and  $\alpha$ -actinin. Intact desmosomes are indicated by white arrowheads. **(B)** Representative double-marker plot of a 3-month-old patient showing flow cytometric analysis of cardiomyocyte cell cycle activity using cardiomyocyte ( $\alpha$ -actinin) and cell cycle (H3P) markers. **(C)** Summary graph showing that patients with heart disease exhibited decreased cell cycling compared to age-matched controls without heart disease. Red dots connected with solid lines indicate results from patients with heart disease, and numbers of corresponding patients are indicated in red. Each donor heart control without heart disease is indicated with an open black symbol connected with dotted lines. Circles represent right ventricular and triangles represent LV samples. Scale bar, 50  $\mu$ m.

is a suitable platform for studies of cardiomyocyte cell cycle stimulation. The 3D culture enabled us to test molecular manipulations that mimic therapeutic interventions and to determine the effect on cardiomyocyte proliferation in situ without disrupting the native myocardial tissue architecture.

Myocardial samples were collected at the time of surgery and maintained for 72 hours with either rNRG1 at 100 ng/ml, the same concentration that stimulated the cycling of cultured cardiomyocytes (22, 29, 30), or fetal calf serum (FCS; 1 or 20%). Tissue samples were subsequently sectioned and stained with antibodies to  $\alpha$ -actinin and H3P (Fig. 7C), and the number of mitotic cardiomyocytes was quantified manually using fluorescence microscopy (Fig. 7D and table S4). Compared with controls (1% FCS;  $n = 8$  hearts studied, all <6 months old), rNRG1 induced an increase in the M-phase cardiomyocyte population in the my-

ocardium by 13- to 31-fold from patients 2 to 5 months of age ( $n = 8$  hearts studied; Fig. 7D and table S4). In samples from 14 patients  $\geq 6$  months of age [age range, 6 months to 66 years (Fig. 7D and table S4)], no M-phase cardiomyocytes were detected. These results indicate that infants with heart disease who are <6 months of age have cardiomyocytes that can be induced with rNRG1 to reenter the cell cycle.

### Infants with heart disease show the capacity for stimulated cardiomyocyte proliferation

We used a nongenetic labeling technique with the fluorescent dye carboxyfluorescein succinimidyl ester (CFSE; fig. S10) to identify proliferating human cardiomyocytes. In the CFSE assay, fluorescein-protein adducts are retained by cells and diluted by half with every cell division. Using our organotypic culture system, we labeled the myocardium with CFSE and identified cardiomyocytes that had divided with the use of flow cytometry and a forward and side scatter gating strategy to enrich for large cells (cardiomyocytes; Fig. 8A, left panel) and to exclude doublets and cell aggregates (Fig. 8A, middle panel) (13); dead cells were excluded with 7-aminoactinomycin D (7-AAD) dye (Fig. 8A, right panel). CFSE populations were quantified in the FL1 channel and revealed two distinct populations (CFSE<sup>lo</sup> and CFSE<sup>hi</sup>). Figure 8B shows representative data from a 3-month-old infant who exhibited a CFSE<sup>lo</sup> population of 4.1%. The CFSE<sup>lo</sup> population represents cardiomyocytes that have undergone several cell divisions, whereas the CFSE<sup>hi</sup> population represents quiescent cardiomyocytes. A CFSE<sup>lo</sup> population was found in every heart (fig. S11). We isolated the CFSE<sup>lo</sup> population for lineage reanalysis and stained it with an isotype antibody to examine the nonspecific binding of the cardiac troponin T (cTnT) antibody (Fig. 8C, left panel); staining with an antibody against cTnT showed that 94.7% of this cell population was cardiomyocytes (Fig. 8C, right panel). These cardiomyocytes had similar forward and side scatter characteristics (Fig. 8D) compared to the original forward and side scatter gate settings (Fig. 8A, left panel). These experiments demonstrate that the CFSE<sup>lo</sup> cells in Fig. 8B are indeed cardiomyocytes.

To further characterize the CFSE<sup>lo</sup> population, we bulk-sorted the cells, isolated RNA, and performed reverse transcription polymerase chain reaction (RT-PCR) analysis to examine the expression of selected marker genes. CFSE<sup>lo</sup> cardiomyocytes expressed the heart-specific markers cTnT and  $\beta$ -myosin heavy chain ( $\beta$ -MHC) but not the stem cell marker *c-Kit*, suggesting that this population contained mature differentiated cardiomyocytes and no dividing stem cells (40) (Fig. 8E). Furthermore, cell cycle-related genes were expressed in the CFSE<sup>lo</sup> but not in the CFSE<sup>hi</sup> population (Fig. 8F). After this extensive validation of the CFSE assay, we examined by flow cytometry the CFSE<sup>lo</sup> population in infant patients with heart disease ( $n = 16$ ). Quantification showed that the CFSE<sup>lo</sup> population was  $5.8 \pm 1.7\%$  ( $n = 4$ ) at 2 months,  $5 \pm 1.4\%$  ( $n = 3$ ) at 3 months, and  $1.2 \pm 0.9\%$  ( $n = 4$ ) at 6 months of age (Fig. 8G and fig. S11). CFSE<sup>lo</sup> populations were not detectable in patients over 6 months of age, indicating that patient age is an important determinant in the proliferative response to rNRG1 (Fig. 8G).

Last, we examined the possibility that rNRG1 stimulation increased the proportion of cardiomyocytes with higher DNA contents, which may arise from DNA synthesis without subsequent nuclear division (endocycling) or nuclear division without subsequent cell division (endomitosis). Addition of rNRG1 did not change the proportion of mononucleated cardiomyocytes (Fig. 8H) or ploidy in the mononucleated portion (Fig. 8I). This supports the conclusion that rNRG1 stimulates cardiomyocyte division in intact infant human myocardium.

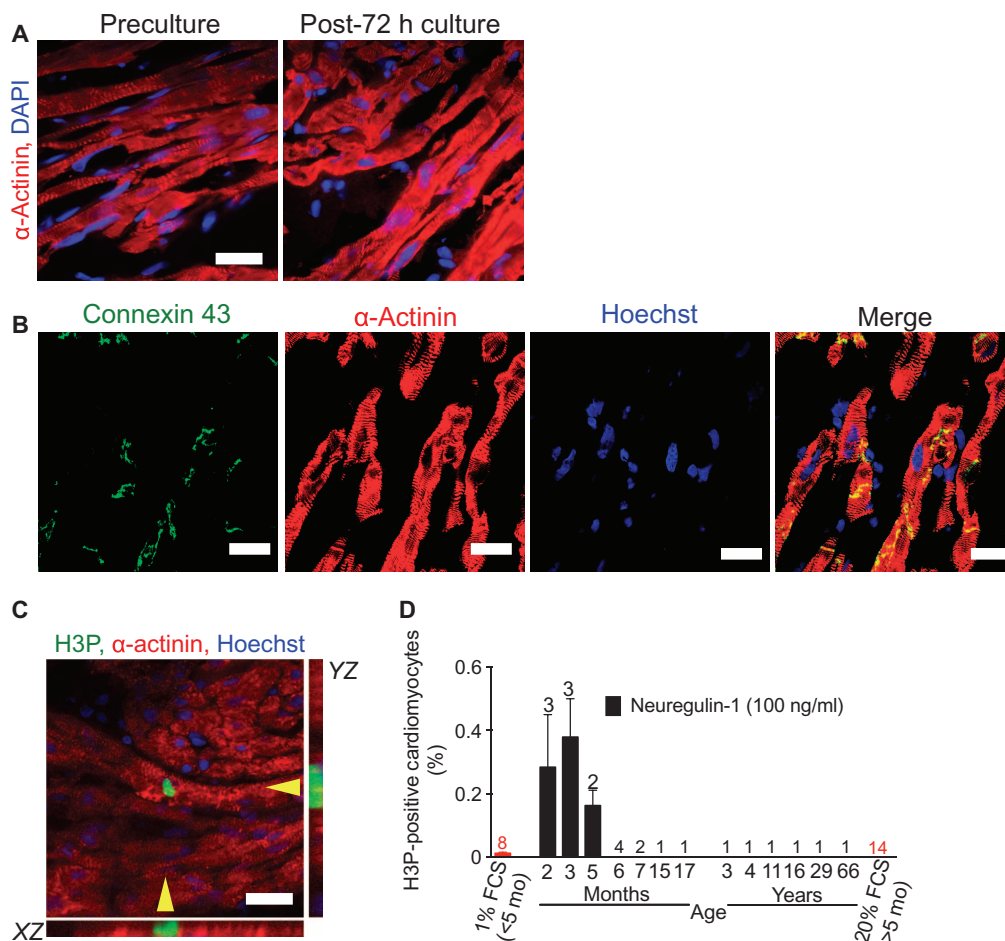


**Fig. 7. rNRG1 stimulates cardiomyocyte cycling in myocardium from infants with heart disease (younger than 6 months of age).** For organotypic culture, chunks of myocardium were maintained in the presence of 1% FCS or rNRG1 for 3 days, fixed, and analyzed by immunofluorescence microscopy. (A and B) Preculture is fresh myocardium. Post-72 hour culture is after 72 hours of organotypic culture. Incubation of cells in organotypic culture for 3 days did not change microscopic architecture (A). Gap junctions and electromechanical connections were identified by connexin 43 staining and were present after 72 hours of organotypic culture (B). (C and D) rNRG1 stimulates cardiomyocytes to enter M phase in a 2-month-old patient with Tetralogy of Fallot. The position of orthogonal reconstructions of the cardiomyocyte in the center are indicated by yellow arrowheads (along the XZ and YZ axes) (C). Quantitative analysis showed that rNRG1 increased M-phase cardiomyocytes in an age-dependent manner (D). Numbers of patients per data point are indicated (D). Scale bars, 20  $\mu$ m (A and C) and 50  $\mu$ m (B).

## DISCUSSION

The findings herein advance a strategy for inducing myocardial repair in pediatric patients. Myocardial regeneration experiments in neonatal mice were not feasible until the recent introduction of techniques for inducing myocardial injury (15, 17, 41). LAD ligation (16, 17) and amputation injury (15, 42) in neonatal mice were reported to lead to scarless repair, although these results are controversial (43, 44). Here, we verify that cryoinjury is a technically feasible method that produces scar formation and dysfunction, which is in line with the scar formation and delayed repair process observed in zebrafish (31–33) and neonatal mice (35, 36) after cryoinjury. We also show that cryoinjury in neonatal mice is a useful model for human infants with heart disease because it recap-

itulates the scar formation, dysfunction, and decrease in cardiomyocyte cell cycle activity frequently seen in young patients with heart disease. The observed decrease in cardiomyocyte proliferation after cryoinjury contrasts with the reported increase in cardiomyocyte cycling after LAD ligation (16) and amputation (15), possibly because of technical differences in the scoring of cardiomyocyte cell cycle events (45). Our results suggest that a population of proliferation-competent cardiomyocytes exists in young mammals and is inhibited or depleted by heart disease. Administration of rNRG1 rescued this inhibition to near-normal levels (about twofold increase) and stimulated the generation of new heart muscle in neonatal mice after cryoinjury and in organotypic cultures of myocardium from infants with heart disease (2 to 5 months of age).

Our model of the mechanisms activated by early administration of rNRG1 in mice involves myocardial protection and regeneration. What are their relative contributions to the overall reparative process? Comparison of the extent of myocardial death between BSA- and rNRG1-treated mice in the early administration group at 1 dpi showed a difference of ~14%, corresponding to ~136,000 cardiomyocytes. On the basis of the H3P analyses, 0.04% of these 136,000 protected cardiomyocytes actively cycle, resulting in ~25,000 new cardiomyocytes over a 34-day period (Supplementary Results). On the other hand, direct quantification of cardiomyocyte nuclear density at 34 dpi revealed  $3.1 \times 10^4$  and  $3.8 \times 10^4$  cardiomyocytes/ $\text{mm}^3$  for BSA- and rNRG1-treated animals, respectively, corresponding to a difference of 7,000 cardiomyocytes/ $\text{mm}^3$ . Subtracting the number of cardiomyocytes contributed by protection, this corresponds to an additional ~224,000 new cardiomyocytes in rNRG1-treated animals in the early administration regimen. From these data, we calculated that the new cardiomyocyte population generated by stimulated proliferation of uninjured cardiomyocytes accounts for 89% [(199,000/224,000)  $\times$  100] and the new cardiomyocyte population generated by proliferation of protected cardiomyocytes accounts for 11% [(25,000/224,000)  $\times$  100] of the total new cardiomyocyte population. We calculated the relative contributions of rNRG1-induced cardiomyocyte protection as 38% [(136,000/(334,000 + 25,000))  $\times$  100], with the remaining 62% resulting from rNRG1-stimulated cardiomyocyte proliferation (Supplementary Results).

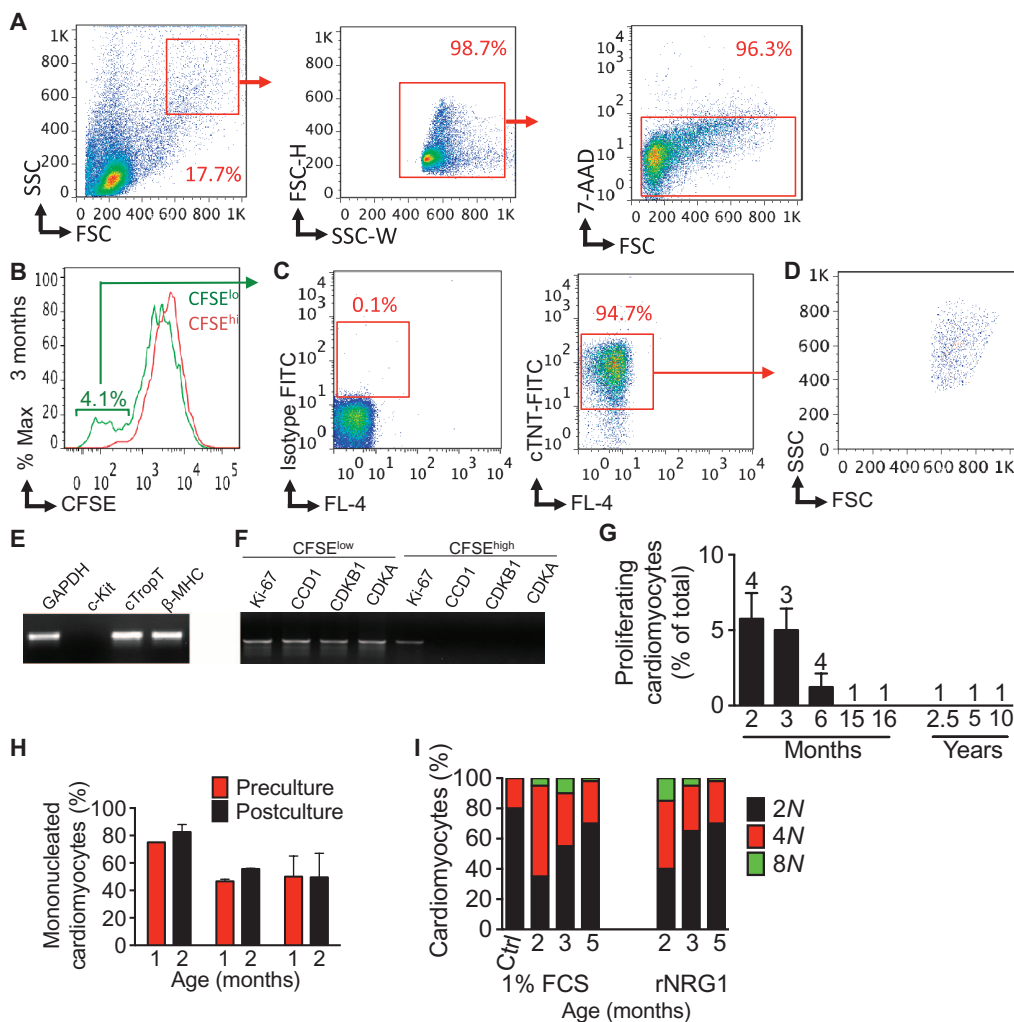


### Fig. 8. rNRG1 stimulates cardiomyocyte proliferation in myocardium from infants with heart disease (younger than 6 months).

Organotypic cultures of human myocardium were metabolically labeled with CFSE and then maintained in the presence of 1% FBS or rNRG1 for 3 days. Cardiomyocytes were analyzed and isolated by fluorescence-activated cell sorting (FACS). (A) FACS strategy for enrichment by size (left panel), doublet discrimination (middle panel), and viability (right panel). (B) Flow cytometric analysis of a 3-month-old infant reveals a CFSE<sup>low</sup> population of 4.1%. (C and D) After fixation, the CFSE<sup>low</sup> population was stained with isotype control (C, left panel) and antibodies against cTnT (C, right panel). Analysis by flow cytometry shows that 94.7% of the population were cardiomyocytes (C, right panel) with forward and side scatter characteristics (D) similar to (A). (E and F) RT-PCR showed that CFSE<sup>low</sup> cardiomyocytes expressed markers of mature differentiated cardiomyocytes (E) and cell cycle-associated genes (F). (G) The graph of proportion of CFSE<sup>low</sup> populations shows that stimulation of cardiomyocyte proliferation in patients with heart disease is age-dependent. Numbers of patients per data point are indicated. (H and I) Laser scanning cytometry shows that administration of rNRG1 in organotypic culture did not change the overall percentage of mononucleated cardiomyocytes (H) or the ploidy pattern of mononucleated cardiomyocytes (I). Red boxes indicate the gating parameters used for data acquisition and analysis (A to D). FSC, forward scatter; SSC, side scatter; FSC-H, forward scatter height; SSC-W, side scatter width; FL4, detector for 488-nm laser with a 695/40 bandpass filter; FITC, fluorescein isothiocyanate; Ctrl, control.

In addition to the increase in the number of cardiomyocytes, rNRG1 might activate other beneficial mechanisms, as suggested by the transient improvement of myocardial function after late administration. The broad range of genes that displayed changes in expression levels after rNRG1 administration (Fig. 5) is consistent with the function of the *NRG1* gene product in sustaining the cardiac gene regulatory network dur-

ing development (19). The rNRG1-regulated genes might hold clues for a deeper understanding of the biological mechanism(s) activated with rNRG1 administration.

The timing of the rNRG1 therapeutic period identified in neonatal mice after cryoinjury was different from that in human infants. In mice, this period ended within the first 5 days of life and is similar to the reported transient period of scarless repair after LAD ligation (16, 17). In humans, this therapeutic window ended at about 6 months of age (Fig. 7D), which is significantly shorter than would have been predicted from our results in humans without heart disease (10). The timing of the rNRG1 therapeutic window in humans leads to two conclusions: (i) administration of rNRG1 in human infants <6 months of age may induce cardiomyocyte regeneration, and (ii) because our mechanistic model involves cardiomyocyte protection, rNRG1 could be administered in infants with congenital heart disease before surgical repair, which is feasible because most of these surgeries are scheduled electively.

It is intriguing to note that human cardiomyocyte cell cycle reentry was not stimulated by rNRG1 in patients older than 6 months (Fig. 7D, Fig. 8G). We demonstrated previously that rNRG1 stimulates cardiomyocyte division in young adult mice (22). Setting aside potential species differences, how could this apparent discrepancy be reconciled? As shown in Fig. 6C, premature cessation of cardiomyocyte cycling occurred in the presence of heart disease, indicating that heart disease in infants drives proliferation-competent cardiomyocytes out of the cell cycle and into a permanently quiescent phenotype. In contrast, the young adult mice characterized in (22) were free from heart disease until 8 weeks of life. In other words, these mice were not exposed to signals that

drive cardiomyocytes prematurely into a permanently quiescent phenotype. It is likely that, as a result, cardiomyocytes with proliferative potential remain present into adulthood and could be stimulated by rNRG1.

Because induction of cardiomyocyte proliferation with rNRG1 appears to be a conserved mechanism in neonatal mice and in myocardium from human infants, targeting the growth factor could represent a therapeutic

strategy for pediatric patients with heart disease. rNRG1 therapy might have risks associated with its proliferative effects in other organs. However, clinical studies that investigate the safety and efficacy of rNRG1 as a cardiac therapeutic in adult patients with heart failure have thus far provided no evidence of uncontrolled growth effects (27, 28). Furthermore, the systemic administration of other recombinant growth factors (for example, insulin, granulocyte-macrophage colony-stimulating factor, erythropoietin, thrombopoietin, and insulin-like growth factor 1) that modify the activity of well-defined signaling pathways is a successful therapeutic paradigm and has a good track record for safety in pediatric patients.

## MATERIALS AND METHODS

### Study design

For the mouse experiments, the study design, including the number of animals to be included and the type and time points of analyses, was predefined by the investigators. Neonatal mouse cryoinjury was performed by B.D.P., and future assignment to rNRG1 and BSA administration was independently performed by B.G. cMRI was performed and analyzed independently by D.G.B. Investigators were blinded with the use of coded samples. Study objects (neonatal mice and human heart samples) were not excluded on the basis of results being outliers. The number of biological and technical replicates is provided in table S9.

### Cryoinjury

Mouse experiments were approved by Boston Children's Hospital and Institute of Molecular Biotechnology. ICR mice were used. Pups born after 5:00 p.m. were considered to be P0 the following day and subjected to cryoablation the next day (P1). Pups received a subcutaneous injection of 0.1% bupivacaine, were placed inside a sleeve, and were put in an ice-water bath until they were nonresponsive to the paw reflex. Ventrolateral thoracotomy was performed between the fourth and fifth ribs, the pericardium was removed, and the heart was exposed. A 1.5-mm diameter vanadium probe was equilibrated in liquid nitrogen for 20 min and applied to the LV epicardium for 2 s. Sham injury consisted of opening the chest and removing the pericardium. The chest was closed with 6-0 Prolene sutures, and the skin was sealed with Webglue (Webster Veterinary) or 8-0 Prolene sutures. Pups recovered under a heating lamp, were placed on a warming blanket until they became responsive, were rubbed with bedding, and were returned to their mothers.

### Visualization of injury by TTC

Freshly excised mouse hearts were washed in ice-cold 50 mM potassium chloride in phosphate-buffered saline (PBS), immediately placed in 1% TTC (w/v; in phosphate buffer, pH 7.4) at 37°C for 20 min, and then fixed in 10% phosphate-buffered formaldehyde overnight. Photomicrographs were taken using a Nikon SMZ1000 stereomicroscope at  $\times 0.8$ ,  $\times 2$ , or  $\times 3$  magnification and an Olympus DP70 charge-coupled device camera.

### Characterization of scar structure and function

We defined a transmural scar as the presence of transmural blue collagen on any of 6 to 12 AFOG-stained sections per heart. We measured the radial thickness of nontransmural scars and remote LV myocardium in diastole and systole on cMRI images using ImageJ and calculated relative systolic thickening as percent systolic change = (length in systole – length in diastole)/length in systole.

### Cardiomyocyte-specific deletion of *ErbB4*

Experiments were performed in  $\alpha$ MHC-MerCreMer<sup>+/+</sup>; ErbB4<sup>F/WT</sup> (control) and in  $\alpha$ MHC-MerCreMer<sup>+/+</sup>; ErbB4<sup>F/F</sup> (test) mice. ErbB4 inactivation was induced with tamoxifen on days P1 to P3 (30  $\mu$ g/g subcutaneously, dissolved in peanut oil). rNRG1 or BSA was administered from P0 for 12 days (P12).

### Quantification of myocardial function in vivo by echocardiography and cMRI

We performed transthoracic echocardiography under anesthesia with a Vevo 2100 device (VisualSonics). cMRI was performed under isoflurane anesthesia with a 9.4-T small-animal MRI scanner (Bruker BioSpin MRI). Details of imaging are provided in Supplementary materials and methods.

### RNAseq sample preparation and data analysis

Total RNA was extracted using the RNeasy Micro kit (Qiagen). Complementary DNA (cDNA) libraries were prepared using the TruSeq Stranded mRNA kit (Illumina). Sequencing was performed on NextSeq 500 instruments (single-strand, single-end indexed, 75 base pairs per read) at a depth of  $35 \times 10^6$  per sample. Single reads were mapped to the mouse genome (m10) using STAR in a strand-specific manner. Cufflinks was used to determine the FPKM (fragments per kilobase of exon per million fragments mapped) levels for each gene from the STAR alignment and was used as input for Cuffdiff. All treatment groups were normalized to sham. Differential gene expression was calculated using Cuffdiff. Read counts were normalized between all samples. Genes with significant change of expression were defined by an adjusted *P* value <0.05 (Maverix Biomics). Functional clustering was performed with DAVID online software. Supplementary Materials and Methods provide additional information.

### Human myocardial samples

Discarded and de-identified human myocardial samples were collected from patients undergoing heart surgery [Institutional Review Board (IRB) protocol #Z06-10-0489]. Clinical information was retrieved through an honest broker (IRB-P00000126). Normal human heart samples, including one fetal heart, were provided by the Sydney Heart Bank at The University of Sydney (Project No: 2012/2814). When known, patients with a 22q11 microdeletion were excluded. For detailed information, please refer to tables S2 to S5.

### Human cardiomyocyte dissociation

Myocardial tissue was washed and resuspended in cold isolation buffer [130 mM NaCl, 5 mM potassium chloride, 1.2 mM monopotassium phosphate, 6 mM Hepes, 5 mM sodium bicarbonate, 1 mM magnesium chloride, and 5 mM glucose (pH 7.4)]. Isolation buffer was supplemented with 0.36 mM calcium chloride for enzyme activity. Cardiac tissue was incubated for 15 to 20 min in isolation buffer supplemented with collagenase IV (Sigma). After each incubation step, the supernatants were transferred into a tube and centrifuged at 600 rpm for 4 min. Cell pellets were resuspended in ice-cold isolation buffer. Several rounds of digestion were performed until the tissue was fully digested.

### Laser scanning cytometry

Myocardial cell preparations were prepared as described above, and laser scanning cytometric analysis for nucleation and ploidy was performed as previously described (10).

### CFSE assay

CFSE is a fluorescein-derived intracellular fluorescent label that is divided between daughter cells upon cell division. Human myocardial samples were washed twice in warm PBS, incubated in PBS/2% FBS containing 0.5  $\mu$ M CFSE (Molecular Probes, C1157) at 37°C for 30 min, and washed with 10 $\times$  volume of ice-cold PBS/2% FBS. Samples were washed once with warm Dulbecco's modified Eagle's medium (DMEM) and incubated in supplemented DMEM for 72 hours. Cardiomyocytes were then isolated as described in "Human cardiomyocyte dissociation" section and analyzed on a FACSAria II (BD Bioscience) in the FL-1 channel. Viable populations were distinguished by 7-AAD. For lineage reanalysis of the CFSE<sup>lo</sup> population, cells were gated according to CFSE-loaded but non-rNRG1-stimulated controls, and 10,000 cells were bulk-sorted into PBS/5% FCS from two patient samples. Cells were fixed in 4% paraformaldehyde (PFA) for 15 min, washed, stained with either primary antibodies to cTnT (Neomarkers) or an isotype control (immunoglobulin G1), and conjugated to FITC fluorophore. Cells were analyzed on a FACSAria II.

### Flow cytometry and FACS

Dissociated cardiomyocytes were prepared as previously described (10), washed, and pelleted for antibody staining. For cell cycle analysis, sarcomeric  $\alpha$ -actinin (Sigma) antibody was conjugated to a FITC secondary antibody and H3P (Upstate) antibody was conjugated to a Pacific Blue secondary antibody (both from Invitrogen, Molecular Probes monoclonal antibody conjugation kits). Cells were fixed in 4% PFA and washed twice with PBS/5% FCS. Cells were stained in PBS/5% FCS and antibody cocktail for 1 hour at 4°C, washed twice, and resuspended in PBS/5% FCS. Samples were acquired on a FACSAria Cell Sorter (BD Biosciences), and data were analyzed with FlowJo software.

### Quantitative RT-PCR

Cardiomyocytes were isolated and sorted with a FACSAria II (100  $\mu$ m nozzle) into TRIzol buffer and were frozen at -80°C. RNA extraction was performed with an RNeasy Micro Kit (Qiagen) according to the manufacturer's instructions, including on-column DNase I digestion. cDNA was synthesized from 200 ng of total RNA. Eluted RNA samples were reverse-transcribed using SuperScript II and random hexamers (Invitrogen). PCR was performed using iQ5 real-time PCR thermal cycler or Bio-Rad CFX384 Touch thermal cycler and iQ SYBR Green Supermix (Bio-Rad) or iTaq Universal SYBR Green Supermix. The normalized values of each biological replicate were averaged before the calculation of fold change in expression levels. The primer sequences are provided in tables S10 and S11.

### Statistical analyses

Numerical results are presented as means  $\pm$  SEM. Statistical testing was performed with Student's *t* test, Fisher's exact test, and ANOVA followed by Bonferroni post hoc testing. Statistical significance was achieved with a two-sided *P* value  $\leq$ 0.05. Statistical analyses were performed with GraphPad Prism, version 6.

### SUPPLEMENTARY MATERIALS

www.sciencetranslationalmedicine.org/cgi/content/full/7/281/281ra45/DC1  
Materials and Methods  
Results

Fig. S1. Contribution of cardiomyocyte proliferation to regeneration.

Fig. S2. Cryoinjured hearts showed loss of sarcomeric organization.

Fig. S3. Characterization of myocardial repair after cryoinjury.

Fig. S4. Transmural scar persists even after 7 months after cryoinjury.

Fig. S5. Visualization of scar and quantification of cardiac function by MRI from early administration group.

Fig. S6. Visualization of scar and quantification of cardiac function by MRI for late administration group.

Fig. S7. Time course of myocardial repair after cryoinjury from early rNRG1 administration group.

Fig. S8. Time course of myocardial repair after cryoinjury from late rNRG1 administration group.

Fig. S9. Failure to visualize transmural scars with late gadolinium enhancement due to low spatial resolution of cMRI in mice.

Fig. S10. Schematic representation illustrating the nongenetic labeling technique with CFSE.

Fig. S11. rNRG1-stimulated cardiomyocyte proliferation in infants is age-dependent (2-month-, 6-month-, 1.5- to 5-year-, and 10-year-old patients).

Table S1. List of all differentially expressed genes between the BSA and rNRG1 treatment groups relative to sham mice (*P* < 0.05).

Table S2. Clinical information of patients with heart disease analyzed for Fig. 6C (H3P activity over age).

Table S3. Clinical information for normal hearts analyzed for Fig. 6C (H3P activity over age).

Table S4. Clinical information of patients with heart disease analyzed for Fig. 7D (rNRG1 stimulation).

Table S5. Clinical information of patients with heart disease analyzed for Fig. 8G (CFSE assay).

Table S6. Comparison of tissue response after cryoinjury in mice and myocardial disease in human infants (myocardial dysfunction, scar formation, and decreased cardiomyocyte cycling).

Table S7. Antibody manufacturers and dilutions.

Table S8. Image acquisition hardware and settings.

Table S9. Quantification of numeric data.

Table S10. Human primers for quantitative RT-PCR for calculation of fold change in expression levels.

Table S11. Mouse primers for quantitative PCR for calculation of fold change in expression levels.

Movie S1. BSA-treated mouse from early administration.

Movie S2. rNRG1-treated mouse from early administration.

Movie S3. BSA-treated mouse from late administration.

Movie S4. rNRG1-treated mouse from late administration.

Movie S5. 3D reconstructions show myocardial syncytium adjacent to the scar after early administration (64 dpi).

Reference (46)

### REFERENCES AND NOTES

1. P. W. Tennant, M. S. Pearce, M. Bythell, J. Rankin, 20-year survival of children born with congenital anomalies: A population-based study. *Lancet* **375**, 649–656 (2010).
2. J. I. Hoffman, S. Kaplan, The incidence of congenital heart disease. *J. Am. Coll. Cardiol.* **39**, 1890–1900 (2002).
3. A. P. Bolger, A. J. Coats, M. A. Gatzoulis, Congenital heart disease: The original heart failure syndrome. *Eur. Heart J.* **24**, 970–976 (2003).
4. K. M. Burns, B. J. Byrne, B. D. Gelb, B. Kühn, L. A. Leinwand, S. Mital, G. D. Pearson, M. Rodefeld, J. W. Rossano, B. L. Stauffer, M. D. Taylor, J. A. Towbin, A. N. Redington, New mechanistic and therapeutic targets for pediatric heart failure: Report from a National Heart, Lung, and Blood Institute working group. *Circulation* **130**, 79–86 (2014).
5. R. E. Shaddy, M. M. Boucek, D. T. Hsu, R. J. Boucek, C. E. Canter, L. Mahony, R. D. Ross, E. Pahl, E. D. Blume, D. A. Dodd, D. N. Rosenthal, J. Burr, B. LaSalle, R. Holubkov, M. A. Lukas, L. Y. Tani; Pediatric Carvedilol Study Group, Carvedilol for children and adolescents with heart failure: A randomized controlled trial. *JAMA* **298**, 1171–1179 (2007).
6. D. T. Hsu, V. Zak, L. Mahony, L. A. Sleeper, A. M. Atz, J. C. Levine, P. C. Barker, C. Ravishanker, B. W. McCrindle, R. V. Williams, K. Altmann, N. S. Ghanayem, R. Margossian, W. K. Chung, W. L. Border, G. D. Pearson, M. P. Stylianou; Pediatric Heart Network Investigators, S. Mital, Enalapril in infants with single ventricle: Results of a multicenter randomized trial. *Circulation* **122**, 333–340 (2010).
7. J. C. Garbern, R. T. Lee, Cardiac stem cell therapy and the promise of heart regeneration. *Cell Stem Cell* **12**, 689–698 (2013).
8. Z. Lin, W. T. Pu, Strategies for cardiac regeneration and repair. *Sci. Transl. Med.* **6**, 239rv1 (2014).
9. O. Bergmann, R. D. Bhardwaj, S. Bernard, S. Zdunek, F. Barnabé-Heider, S. Walsh, J. Zupicich, K. Alkass, B. A. Buchholz, H. Druid, S. Jovinge, J. Frisén, Evidence for cardiomyocyte renewal in humans. *Science* **324**, 98–102 (2009).
10. M. Mollova, K. Bersell, S. Walsh, J. Savla, L. T. Das, S. Y. Park, L. E. Silberstein, C. G. Dos Remedios, D. Graham, S. Colan, B. Kühn, Cardiomyocyte proliferation contributes to heart growth in young humans. *Proc. Natl. Acad. Sci. U.S.A.* **110**, 1446–1451 (2013).

11. M. H. Soonpaa, K. K. Kim, L. Pajak, M. Franklin, L. J. Field, Cardiomyocyte DNA synthesis and binucleation during murine development. *Am. J. Physiol.* **271**, H2183–H2189 (1996).
12. F. Li, X. Wang, J. M. Capasso, A. M. Gerdes, Rapid transition of cardiac myocytes from hyperplasia to hypertrophy during postnatal development. *J. Mol. Cell. Cardiol.* **28**, 1737–1746 (1996).
13. S. Walsh, A. Ponten, B. K. Fleischmann, S. Jovinge, Cardiomyocyte cell cycle control and growth estimation in vivo—An analysis based on cardiomyocyte nuclei. *Cardiovasc. Res.* **86**, 365–373 (2010).
14. N. Naqvi, M. Li, J. W. Calvert, T. Tejada, J. P. Lambert, J. Wu, S. H. Kesteven, S. R. Holman, T. Matsuda, J. D. Lovelock, W. W. Howard, S. E. Iismaa, A. Y. Chan, B. H. Crawford, M. B. Wagner, D. I. Martin, D. J. Lefer, R. M. Graham, A. Husain, A proliferative burst during preadolescence establishes the final cardiomyocyte number. *Cell* **157**, 795–807 (2014).
15. E. R. Porrello, E. I. Mahmoud, E. Simpson, J. A. Hill, J. A. Richardson, E. N. Olson, H. A. Sadek, Transient regenerative potential of the neonatal mouse heart. *Science* **331**, 1078–1080 (2011).
16. E. R. Porrello, A. I. Mahmoud, E. Simpson, B. A. Johnson, D. Grinsfelder, D. Canseco, P. P. Mammen, B. A. Rothmel, E. N. Olson, H. A. Sadek, Regulation of neonatal and adult mammalian heart regeneration by the miR-15 family. *Proc. Natl. Acad. Sci. U.S.A.* **110**, 187–192 (2013).
17. B. J. Haubner, M. Adamowicz-Brice, S. Khadayate, V. Tiefenthaler, B. Metzler, T. Aitman, J. M. Penninger, Complete cardiac regeneration in a mouse model of myocardial infarction. *Aging* **4**, 966–977 (2012).
18. D. Meyer, C. Birchmeier, Multiple essential functions of neuregulin in development. *Nature* **378**, 386–390 (1995).
19. D. Lai, A. Forrai, X. Liu, O. Wolstein, J. Michalicki, I. Ahmed, A. N. Garratt, C. Birchmeier, M. Zhou, L. Hartley, L. Robb, M. P. Feneley, D. Fatkin, R. P. Harvey, Neuregulin 1 sustains the gene regulatory network in both trabecular and nontrabecular myocardium. *Circ. Res.* **107**, 715–727 (2010).
20. N. Hedhli, Q. Huang, A. Kalinowski, M. Palmeri, X. Hu, R. R. Russell, K. S. Russell, Endothelium-derived neuregulin protects the heart against ischemic injury. *Circulation* **123**, 2254–2262 (2011).
21. X. Liu, X. Gu, Z. Li, X. Li, H. Li, J. Chang, P. Chen, J. Jin, B. Xi, D. Chen, D. Lai, R. M. Graham, M. Zhou, Neuregulin-1/erbB-activation improves cardiac function and survival in models of ischemic, dilated, and viral cardiomyopathy. *J. Am. Coll. Cardiol.* **48**, 1438–1447 (2006).
22. K. Bersell, S. Arab, B. Haring, B. Kühn, Neuregulin1/ErbB4 signaling induces cardiomyocyte proliferation and repair of heart injury. *Cell* **138**, 257–270 (2009).
23. S. M. Jay, A. C. Murthy, J. F. Hawkins, J. R. Wortzel, M. L. Steinhauser, L. M. Alvarez, J. Gannon, C. A. Macrae, L. G. Griffith, R. T. Lee, An engineered bivalent neuregulin protects against doxorubicin-induced cardiotoxicity with reduced proneoplastic potential. *Circulation* **128**, 152–161 (2013).
24. J. E. Cohen, B. P. Purcell, J. W. MacArthur Jr., A. Mu, Y. Shudo, J. B. Patel, C. M. Brusalis, A. Trubelja, A. S. Fairman, B. B. Edwards, M. S. Davis, G. Hung, W. Hiesinger, P. Atluri, K. B. Margulies, J. A. Burdick, Y. J. Woo, A bioengineered hydrogel system enables targeted and sustained intramyocardial delivery of neuregulin, activating the cardiomyocyte cell cycle and enhancing ventricular function in a murine model of ischemic cardiomyopathy. *Circ. Heart Fail.* **7**, 619–626 (2014).
25. B. Wadugu, B. Kühn, The role of neuregulin/ErbB2/ErbB4 signaling in the heart with special focus on effects on cardiomyocyte proliferation. *Am. J. Physiol. Heart Circ. Physiol.* **302**, H2139–H2147 (2012).
26. E. M. Parodi, B. Kuhn, Signalling between microvascular endothelium and cardiomyocytes through neuregulin. *Cardiovasc. Res.* **102**, 194–204 (2014).
27. R. Gao, J. Zhang, L. Cheng, X. Wu, W. Dong, X. Yang, T. Li, X. Liu, Y. Xu, X. Li, M. Zhou, A phase II, randomized, double-blind, multicenter, based on standard therapy, placebo-controlled study of the efficacy and safety of recombinant human neuregulin-1 in patients with chronic heart failure. *J. Am. Coll. Cardiol.* **55**, 1907–1914 (2010).
28. A. Jabbour, C. S. Hayward, A. M. Keogh, E. Kotlyar, J. A. McCrohon, J. F. England, R. Amor, X. Liu, X. Y. Li, M. D. Zhou, R. M. Graham, P. S. Macdonald, Parenteral administration of recombinant human neuregulin-1 to patients with stable chronic heart failure produces favourable acute and chronic haemodynamic responses. *Eur. J. Heart Fail.* **13**, 83–92 (2011).
29. Y. Y. Zhao, D. R. Sawyer, R. R. Baliga, D. J. Opel, X. Han, M. A. Marchionni, R. A. Kelly, Neuregulins promote survival and growth of cardiac myocytes. Persistence of ErbB2 and ErbB4 expression in neonatal and adult ventricular myocytes. *J. Biol. Chem.* **273**, 10261–10269 (1998).
30. F. B. Engel, M. Schebesta, M. T. Duong, G. Lu, S. Ren, J. B. Madwed, H. Jiang, Y. Wang, M. T. Keating, p38 MAP kinase inhibition enables proliferation of adult mammalian cardiomyocytes. *Genes Dev.* **19**, 1175–1187 (2005).
31. F. Chablais, J. Veit, G. Rainer, A. Jaźwińska, The zebrafish heart regenerates after cryoinjury-induced myocardial infarction. *BMC Dev. Biol.* **11**, 21 (2011).
32. K. Schnabel, C. C. Wu, T. Kurth, G. Weidinger, Regeneration of cryoinjury induced necrotic heart lesions in zebrafish is associated with epicardial activation and cardiomyocyte proliferation. *PLOS One* **6**, e18503 (2011).
33. J. M. González-Rosa, V. Martin, M. Peralta, M. Torres, N. Mercader, Extensive scar formation and regression during heart regeneration after cryoinjury in zebrafish. *Development* **138**, 1663–1674 (2011).
34. J. M. González-Rosa, N. Mercader, Cryoinjury as a myocardial infarction model for the study of cardiac regeneration in the zebrafish. *Nat. Protoc.* **7**, 782–788 (2012).
35. S. A. Jesty, M. A. Steffey, F. K. Lee, M. Breitbart, M. Hesse, S. Reining, J. C. Lee, R. M. Doran, A. Y. Nikitin, B. K. Fleischmann, M. I. Kotlikoff, c-kit<sup>+</sup> precursors support postinfarction myogenesis in the neonatal, but not adult, heart. *Proc. Natl. Acad. Sci. U.S.A.* **109**, 13380–13385 (2012).
36. A. Darezhereshki, N. Rubin, L. Gamba, J. Kim, J. Fraser, Y. Huang, J. Billings, R. Mohammadzadeh, J. Wood, D. Warburton, V. Kaartinen, C. L. Lien, Differential regenerative capacity of neonatal mouse hearts after cryoinjury. *Dev. Biol.* **399**, 91–99 (2015).
37. A. K. Bose, J. W. Mathewson, B. E. Anderson, A. M. Andrews, A. Martin Gerdes, M. Benjamin Perryman, P. D. Grossfeld, Initial experience with high frequency ultrasound for the newborn C57BL mouse. *Echocardiography* **24**, 412–419 (2007).
38. K. D. Poss, L. G. Wilson, M. T. Keating, Heart regeneration in zebrafish. *Science* **298**, 2188–2190 (2002).
39. M. Brandenburger, J. Wenzel, R. Bogdan, D. Richardt, F. Nguemo, M. Reppel, J. Hescheler, H. Terlau, A. Dendorfer, Organotypic slice culture from human adult ventricular myocardium. *Cardiovasc. Res.* **93**, 50–59 (2012).
40. M. M. Zaruba, M. Soonpaa, S. Reuter, L. J. Field, Cardiomyogenic potential of C-kit<sup>+</sup>-expressing cells derived from neonatal and adult mouse hearts. *Circulation* **121**, 1992–2000 (2010).
41. A. I. Mahmoud, E. R. Porrello, W. Kimura, E. N. Olson, H. A. Sadek, Surgical models for cardiac regeneration in neonatal mice. *Nat. Protoc.* **9**, 305–311 (2014).
42. D. M. Bryant, C. C. O'Meara, N. N. Ho, J. Gannon, L. Cai, R. T. Lee, A systematic analysis of neonatal mouse heart regeneration after apical resection. *J. Mol. Cell. Cardiol.* **79**, 315–318 (2015).
43. D. C. Andersen, S. Ganesalingam, C. H. Jensen, S. P. Sheikh, Do neonatal mouse hearts regenerate following heart apex resection? *Stem Cell Reports* **2**, 406–413 (2014).
44. T. Konfino, N. Landa, T. Ben-Mordechai, J. Leor, The type of injury dictates the mode of repair in neonatal and adult heart. *J. Am. Heart Assoc.* **4**, e001320 (2015).
45. K. L. Ang, L. T. Shenje, S. Reuter, M. H. Soonpaa, M. Rubart, L. J. Field, M. Galiñanes, Limitations of conventional approaches to identify myocyte nuclei in histologic sections of the heart. *Am. J. Physiol. Cell Physiol.* **298**, C1603–C1609 (2010).
46. J. Frahm, A. Haase, D. Matthaei, Rapid NMR imaging of dynamic processes using the FLASH technique. *Magn. Reson. Med.* **3**, 321 (1986).

**Acknowledgments:** We thank H. Sadek and M. Ahmad (University of Texas Southwestern, Dallas) for the training in mouse surgery; M. Farley and D. Burstein [Beth Israel Deaconess Medical Center (BIDMC), Boston, MA] for their help with cMRI; the members of the Kuhn laboratory for helpful discussions; the cardiac surgeons at Boston Children's Hospital for providing de-identified human myocardium (F. Pigula, F. Fynn-Thompson, S. Emani, J. Mayer, C. Baird, and P. Del Nido); E. McCusky (Boston Children's Hospital) for retrieval of clinical information; the staff at the laser scanning cytometer core at the Department of Transfusion Medicine (Boston Children's Hospital), especially L. Silberstein and S.-Y. Park; N. Francis and D. Bennett (Boston Children's Hospital) for FACS assistance; and W. Home and A. Ferguson (Rangos Genomics Facility at Children's Hospital of Pittsburgh of UPMC) for their assistance with RNAseq. **Funding:** This research was supported by the Department of Cardiology and the Translational Research Program at Boston Children's Hospital and NIH grants R01HL106302 and K08HL085143 (to B.K.). B.D.P. and S.C. were supported by the Office of Faculty Development (Boston Children's Hospital), and B.D.P. by T32HL007572 from the NIH. S.W. received an AHA postdoctoral fellowship award. We acknowledge support from an NIH instrumentation grant (RR028792) to BIDMC Boston, MA. B.G., N.A., and B.K. were supported by the Richard King Mellon Institute for Pediatric Research (Children's Hospital of Pittsburgh of UPMC). J.M.P. and B.J.H. were funded by a Fondation Leducq Transatlantic Network of Excellence Award. **Author contributions:** B.D.P., B.G., S.W., S.C., B.J.H., C.G.R., J.M.P., and B.K. developed the research strategy. B.D.P., B.G., S.C., N.A., D.G.B., and B.J.H. designed, performed, and analyzed the animal experiments. S.W., S.C., and N.A. designed, performed, and analyzed the experiments with human heart samples. C.G.R. provided nondiseased human heart tissue. B.D.P., B.G., S.W., and B.K. wrote and all authors edited the manuscript. **Competing interests:** The authors declare that they have no competing interests.

Submitted 18 December 2014

Accepted 27 February 2015

Published 1 April 2015

10.1126/scitranslmed.aaa5171

**Citation:** B. D. Polizzotti, B. Ganapathy, S. Walsh, S. Choudhury, N. Ammanamanchi, D. G. Bennett, C. G. dos Remedios, B. J. Haubner, J. M. Penninger, B. Kühn, Neuregulin stimulation of cardiomyocyte regeneration in mice and human myocardium reveals a therapeutic window. *Sci. Transl. Med.* **7**, 281ra45 (2015).

Editor's Summary

### Young at heart: Restoring cardiac function in children

When children are given adult roles in TV commercials, the results range from adorable to brilliant to simply hilarious. But when children with heart disease were given adult medicines in clinical trials, the results were disappointing—and the need for pediatric-specific treatment regimens became clear. In adult mice, the recombinant growth factor neuregulin-1 (rNRG1) stimulates heart regeneration by driving the proliferation of heart muscle cells (cardiomyocytes). Because young mice bear more proliferation-competent cardiomyocytes than do adult animals, Polizzotti *et al.* asked whether rNRG1 might put cardiomyocyte proliferation into overdrive if given to mice during the neonatal period. To test their hypothesis, the authors treated newborn mice with rNRG1 at various times after heart injury and found that early treatment starting at 1 day of age boosted cardiomyocyte cell division and heart function in a persistent manner relative to treatment regimens that began at 4 days after birth. rNRG1 also drove cardiomyocyte proliferation in heart muscle isolated from human infants with heart disease who were less than 6 months of age, but not in tissue from older pediatric patients. These findings suggest that rNRG1 administration during the neonatal period might be a new therapeutic strategy for pediatric heart disease. Now that would be brilliant.

**A complete electronic version of this article** and other services, including high-resolution figures, can be found at:

<http://stm.sciencemag.org/content/7/281/281ra45.full.html>

**Supplementary Material** can be found in the online version of this article at:

<http://stm.sciencemag.org/content/suppl/2015/03/30/7.281.281ra45.DC1.html>

**Related Resources for this article** can be found online at:

<http://stm.sciencemag.org/content/scitransmed/6/227/227fs11.full.html>

<http://stm.sciencemag.org/content/scitransmed/4/154/154ra135.full.html>

<http://stm.sciencemag.org/content/scitransmed/6/239/239rv1.full.html>

<http://stm.sciencemag.org/content/scitransmed/6/224/224ra27.full.html>

<http://stm.sciencemag.org/content/scitransmed/5/196/196ra99.full.html>

Information about obtaining **reprints** of this article or about obtaining **permission to reproduce this article** in whole or in part can be found at:

<http://www.sciencemag.org/about/permissions.dtl>